Supporting information for

Catalytic N_2-to-NH_3 Conversion by Fe at Lower Driving Force: A Proposed Role for Metallocene-Mediated PCET

Matthew J. Chalkley,[†] Trevor J. Del Castillo,[†] Benjamin D. Matson,[†] Joseph P. Roddy and Jonas C. Peters*

[†]M.J.C., T.J.D.C. and B.D.M. contributed equally to this work.

Division of Chemistry and Chemical Engineering, California Institute of Technology, Pasadena, California 91125, United States

Table of Contents:

1. Experimental details

1.1 General considerations:

All manipulations were carried out using standard Schlenk or glovebox techniques under an N_2 atmosphere. Solvents were deoxygenated and dried by thoroughly sparging with N_2 followed by passage through an activated alumina column in a solvent purification system by SG Water, USA LLC. Non-halogenated solvents were tested with sodium benzophenone ketyl in tetrahydrofuran (THF) in order to confirm the absence of oxygen and water. Deuterated solvents were purchased from Cambridge Isotope Laboratories, Inc., degassed, and dried over activated 3-Å molecular sieves prior to use.

Cp^*_2Co,[1] $[P_3^BFe][BAr^F_4]$,[2] $P_3^{Si}FeN_2$,[3] $[P_3^BCoN_2][Na(12\text{-crown-}4)_2]$,[4] $P_3^{Si}CoN_2$,[5] $[P_3^BFeN_2][Na(12\text{-crown-}4)_2]$,[6] and $[Ph_2{}^{15}NH_2][OTf]$[7,8] were prepared according to literature procedures. $Ph^{15}NH_2$ was obtained from Sigma-Aldrich, Inc. degassed, and dried over activated 3-Å molecular sieves prior to use**.** All other reagents were purchased from commercial vendors and used without further purification unless otherwise stated. Diethyl ether (Et_2O) used in the experiments herein was stirred over Na/K ($\geq$ 2 hours) and filtered or vacuum-transferred before use unless otherwise stated.

1.2 Physical Methods:

^1H chemical shifts are reported in ppm relative to tetramethylsilane, using ^1H resonances from residual solvent as internal standards. IR measurements were obtained as solutions or thin films formed by evaporation of solutions using a Bruker Alpha Platinum ATR spectrometer with OPUS software (solution IR collected in a cell with KBr windows and a 1 mm pathlength). H_2 was quantified on an Agilent 7890A gas chromatograph (HP-PLOT U, 30 m, 0.32 mm ID; 30 °C isothermal; nitrogen carrier gas) using a thermal conductivity detector.

1.3 Mössbauer Spectroscopy:

Mössbauer spectra were recorded on a spectrometer from SEE Co. (Edina, MN) operating in the constant acceleration mode in a transmission geometry. The sample was kept in an SVT-400 cryostat form Janis (Wilmington, MA). The quoted isomer shifts are relative to the centroid of the spectrum of a metallic foil of α-Fe at room temperature (RT). Solution samples were transferred to a sample cup and chilled to 77 K inside of the glovebox, and unless noted otherwise, quickly removed from the glovebox and immersed in liquid N_2 until mounted in the cryostat. Data analysis was performed using version 4 of the program WMOSS (www.wmoss.org) and quadrupole doublets were fit to Lorentzian lineshapes. See discussion below for detailed notes on the fitting procedure.

1.4 Ammonia and Hydrazine Quantification:

Reaction mixtures are cooled to 77 K and allowed to freeze. The reaction vessel is then opened to atmosphere and to the frozen solution is slowly added an excess (with respect to acid) solution of a NaO^tBu solution in MeOH (0.25 mM) over 1-2 minutes. This solution is allowed to freeze, then the headspace of the tube is evacuated and the tube is sealed. The tube is then allowed to warm to RT and stirred at RT for at least 10 minutes. An additional Schlenk tube is charged with HCl (3 mL of a 2.0 M solution in Et_2O, 6 mmol) to serve as a collection flask. The volatiles of the reaction mixture are vacuum transferred at RT into this collection flask. After completion of the vacuum transfer, the collection flask is sealed and warmed to RT. Solvent is removed in vacuo, and the remaining residue is dissolved in H_2O (1 mL). An aliquot of this solution (10–100 μL) is then analyzed for the presence of NH_3 (present as NH_4Cl) by the indophenol method.[9] A further aliquot of this solution is analyzed for the presence of N_2H_4 (present as N_2H_5Cl) by a standard colorimetric method.[10] Quantification is performed with UV−vis spectroscopy by analyzing absorbance at 635 nm. In this case of runs with $[PhNH_3][OTf]$ we found that aniline in the form of anilinium chloride was present in the receiving vessels. The anilinium chloride interfered with the indophenol and hydrazine detection method. Therefore, quantification for NH_3 was performed by extracting the solid residue into 1 mL of DMSO-d_6 that has 20 mmol of trimethoxybenzene as an internal standard. Integration of the ^1H NMR peak observed for NH_4 was then integrated against the two peaks of

trimethoxybenzene to quantify the ammonium present. This ^{1}H NMR detection method was also used to differentiate [$^{14}NH_4$][Cl] and [$^{15}NH_4$][Cl] produced in the control reactions conducted with [$^{15}NPh_2H_2$][OTf].

1.5 EPR Spectroscopy

X-band EPR spectra were obtained on a Bruker EMX spectrometer. Samples were collected at powers ranging from 6-7 mW with modulation amplitudes of 2.00 G, modulation frequencies of 100.00 kHz, over a range of 1800 to 4500 Gauss. Spectra were baseline corrected using the algorithm in SpinCount.[11] EPR spectra were modeled using the easyspin program.[12]

1.6 Computational Methods

All stationary point geometries were calculated using DFT with an M06-L functional,[13] a def2-TZVP[14] basis set on transition metals (Stuttgart ECP[15] was used on Mo atoms) and a def2-SVP[14] basis set on all other atoms. Calculations were performed, in part, using Xtreme Science and Engineering Discovery Environment (XSEDE) resources.[16] Calculations were performed on the full P_3^EFe scaffolds. Calculations on the [HIPTN$_3$N]Mo system were performed on a truncated scaffold in which the isopropyl groups were removed (i.e. [{3,5-$(C_6H_4)_2C_6H_3NCH_2CH_2\}_3N]^{3-}$). Geometries were optimized using the NWChem 6.5 package.[17] All single point energy, frequency and solvation energy calculations were performed with the Gaussian09 package.[18] Frequency calculations were used to confirm true minima and to determine gas phase free energy values (G_{gas}). Single point solvation calculations were done using an SMD solvation model with diethyl ether solvent and were used to determine solvated internal energy (E_{soln}). Free energies of solvation were approximated using the difference in gas phase internal energy (E_{gas}) and solvated internal energy ($\Delta G_{solv} \approx E_{soln} - E_{gas}$) and the free energy of a species in solution was then calculated using the gas phase free energy (G_{gas}) and the free energy of solvation ($G_{soln} = G_{gas} + \Delta G_{solv}$).[19,20,21] All reduction potentials were calculated referenced to $Fc^{+/0}$ using the standard Nernst relation $\Delta G = -nFE^0$.

1.7 Gas Chromatography

H2 was quantified on an HP 5890 Series II Plus Gas Chromatograph (nitrogen carrier gas) using a thermal conductivity detector. All measurements were obtained using a 100 µL manual injection and the final value was obtained as an average of two runs.

2. Synthetic Details:

2.1 General Procedure for the Synthesis of the Acids:

Prior to use the amine was purified (aniline by distillation and diphenylamine by recrystallization). To a 250 mL round bottom flask in the glovebox was added the amine which was subsequently dissolved in 100 mL of Et_2O (no additional drying with NaK). To this was added dropwise (1 equiv) of HOTf with stirring over five minutes. Immediate precipitation of white solid was observed and the reaction mixture was allowed to stir for one hour at RT. The reaction mixture was then filtered and the resulting white powder was washed with Et_2O (50 mL), pentane (50 mL) and Et_2O again (50 mL). The resulting white microcrystalline material was then dried under vacuum. Yields of greater than 90% of microcrystalline material was obtained in this manner in all cases.

2.2 Procedure for Reaction of Cp^*_2Co with Acid:

A 1 mL solution of HOTf or DOTf (23 µL, 3.0 eq) in toluene and a 2 mL solution of Cp^*_2Co (40 mg, 1.0 eq) was chilled to -78 °C for ten minutes in a cold well. With strong stirring the Cp^*_2Co solution was added dropwise over ten minutes to the HOTf solution. Purple precipitate could be observed upon the

addition of each drop. After the completion of the addition the reaction mixture was allowed to stir for 5 more minutes. The reaction was then vacuum filtered in the cold well through a medium porosity frit to yield a purple solid. This solid was then washed with toluene that had been prechilled to -78 °C (5 mL) and then likewise prechilled pentane (15 mL). After drying on the frit for ten minutes the solid was then transferred to a prechilled vial. The solid was then dried under vacuum for several hours at -78 °C. Exact yields were not obtained due to the solid retaining some solvent even after extended drying at these temperatures; however, the material isolated reproducibly represents > 75% of the expected chemical yield. All further spectroscopic and reactivity characterization of this material was carried out immediately after its synthesis and with the maintenance of the material at ≤ -78 °C except where specifically noted.

3. Ammonia production and quantification studies

3.1 Standard NH_3 Generation Reaction Procedure:

All solvents are stirred with Na/K for ≥2 hours and filtered prior to use. In a nitrogen-filled glovebox, the precatalyst (2.3 μmol) was weighed into a vial.* The precatalyst was then transferred quantitatively into a Schlenk tube using THF. The THF was then evaporated to provide a thin film of precatalyst at the bottom of the Schlenk tube. The tube is then charged with a stir bar and the acid and reductant are added as solids. The tube is then cooled to 77 K in a cold well. To the cold tube is added Et_2O to produce a concentration of precatalyst of 2.3 mM. The temperature of the system is allowed to equilibrate for 5 minutes and then the tube is sealed with a Teflon screw-valve. This tube is passed out of the box into a liquid N_2 bath and transported to a fume hood. The tube is then transferred to a dry ice/acetone bath where it thaws and is allowed to stir at -78 °C for three hours. At this point the tube is allowed to warm to RT with stirring, and stirred at RT for 5 minutes. To ensure reproducibility, all experiments were conducted in 200 mL Schlenk tubes (51 mm OD) using 25 mm stir bars, and stirring was conducted at ~900 rpm.

* In cases where less than 2.3 μmol of precatalyst was used stock solutions were used to avoid having to weigh very small amounts.

Table S1: UV-vis quantification results for standard NH_3 generation experiments with $P_3^BFe^+$

Entry	$P_3^BFe^+$ (μmol)	Acid equiv	Cp^*_2Co equiv	NH_4Cl (μmol)	N_2H_5Cl (μmol)	Equiv NH_3/Fe	% Yield NH_3 Based on e^-
A	2.3	108[a]	54	31.4	0.0	13.5	75.6
B	2.3	108[a]	54	28.5	0.0	12.3	68.6
C	2.3	108[a]	54	29.2	0.0	12.6	70.4
Avg.						12.8 ± 0.5	72 ± 3
D	2.3	322[a]	162	76.4	2.0	33.0	61.4
E	2.3	322[a]	162	80.0	0.7	34.5	64.2
Avg.						34 ± 1	63 ± 2
F	2.3	638[a]	322	60.4	0.5	26.0	24.3
G	2.3	638[a]	322	63.2	0.3	27.3	25.4
Avg.						26.7 ± 0.9	25 ± 1
H	1.1	108[b]	54	7.8	0.0	6.9	37.6
I	2.3	108[b]	54	19.2	0.0	8.3	46.3
Avg.						8 ± 1	42 ± 6
J	2.3	108[c]	54	17.7	N.D.	7.7	43.1
K	2.3	108[c]	54	13.8	N.D.	6.0	33.6

Avg.						7 ± 1	38 ± 7
L	2.3	322[c]	162	39.8	N.D.	17.3	32.0
M	2.3	322[c]	162	31.9	N.D.	13.9	25.7
Avg.						16 ± 3	29 ± 4

N.D. indicates the value was not determined [a]Acid used is $[Ph_2NH_2][OTf]$ [b]Acid used is $[Ph_2NH_2][BAr^F{}_4]$ [c]Acid used is $[PhNH_3][OTf]$

Table S2: UV-vis quantification results for standard NH_3 generation experiments with $P_3{}^{Si}FeN_2$

Entry	$P_3{}^{Si}FeN_2$ (µmol)	Acid equiv	Cp^*_2Co equiv	NH_4Cl (µmol)	N_2H_5Cl (µmol)	Equiv NH_3/Fe	% Yield NH_3 Based on e^-
A	2.3	108[a]	54	6.6	0.0	1.7	9.3
B	2.3	108[a]	54	2.7	0.0	0.7	3.8
Avg.						1.2 ± 0.2	6.5 ± 0.3

[a]Acid used is $[Ph_2NH_2][OTf]$

Table S3: UV-vis quantification results for standard NH_3 generation experiments with $P_3{}^{B}CoN_2^-$

Entry	$P_3{}^{B}CoN_2^-$ (µmol)	Acid equiv	Cp^*_2Co equiv	NH_4Cl (µmol)	N_2H_5Cl (µmol)	Equiv NH_3/Fe	% Yield NH_3 Based on e^-
A	2.3	108[a]	54	3.0	0.0	1.3	7.2
B	2.3	108[a]	54	1.8	0.0	0.8	4.4
Avg.						1.1 ± 0.4	6 ± 2

[a]Acid used is $[Ph_2NH_2][OTf]$

Table S4: UV-vis quantification results for standard NH_3 generation experiments with $P_3{}^{Si}CoN_2$

Entry	$P_3{}^{Si}CoN_2$ (µmol)	Acid equiv	Cp^*_2Co equiv	NH_4Cl (µmol)	N_2H_5Cl (µmol)	Equiv NH_3/Fe	% Yield NH_3 Based on e^-
A	2.3	108[a]	54	0.0	0.0	0.0	0.0
B	2.3	108[a]	54	0.0	0.0	0.0	0.0
Avg.						0.0	0.0

[a]Acid used is $[Ph_2NH_2][OTf]$

3.2 Ammonia production studies with $[Ph_2{}^{15}NH_2][OTf]$:

The procedure was the same as the general procedure presented in section 3.1 with 2.3 µmol of $P_3{}^{B}Fe^+$ catalyst, 54 equiv Cp^*_2Co, and 108 equiv $[Ph_2{}^{15}NH_2][OTf]$. Product analyzed by ^1H NMR as described in section 1.4 and only the diagnostic triplet of $[^{14}NH_4][Cl]$ is observed.

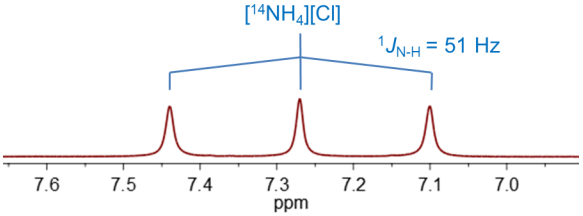

Figure S1: ^{1}H NMR spectrum (300 MHz, DMSO-d_6) of [$^{14}NH_4$][Cl] produced from catalytic N_2-to-NH_3 conversion conducted with $P_3^BFe^+$ catalyst, 54 equiv Cp^*_2Co, and 108 equiv [$Ph_2{}^{15}NH_2$][OTf] under an atmosphere of $^{14}N_2$.

4. NH_3 Generation Reaction with Periodic Substrate Reloading – Procedure with $P_3^BFe^+$:

All solvents are stirred with Na/K for ≥2 hours and filtered prior to use. In a nitrogen-filled glovebox, the precatalyst (2.3 μmol) was weighed into a vial. The precatalyst was then transferred quantitatively into a Schlenk tube using THF. The THF was then evaporated to provide a thin film of precatalyst at the bottom of the Schlenk tube. The tube is then charged with a stir bar and the acid and reductant are added as solids. The tube is then cooled to 77 K in a cold well. To the cold tube is added 1 mL of Et_2O. The temperature of the system is allowed to equilibrate for 5 minutes and then the tube is sealed with a Teflon screw-valve. The cold well cooling bath is switched from a $N_{2(l)}$ bath to a dry ice/acetone bath. In the cold well the mixture in the sealed tube thaws with stirring and is allowed to stir at -78 °C for 3 hours. Then, without allowing the tube to warm above -78 °C, the cold well bath is switched from dry ice/acetone to $N_{2(l)}$. After fifteen minutes the reaction mixture is observed to have frozen, at this time the tube is opened. To the cold tube is added acid (324 equiv) and reductant (162 equiv) as solids. To the tube then 1 additional mL of Na/K-dried Et_2O is added. The cold well cooling bath is switched from a $N_{2(l)}$ bath to a dry ice/acetone bath. In the cold well the mixture in the sealed tube thaws with stirring and is allowed to stir at -78 °C for 3 hours. These reloading steps are repeated the desired number of times. Then the tube is allowed to warm to RT with stirring, and stirred at RT for 5 minutes.

Table S5: UV-vis quantification results for NH_3 generation experiments with $P_3^BFe^+$, with reloading

Entry	Number of Loadings	$P_3^BFe^+$ (μmol)	Acid equiv	Cp^*_2Co equiv	NH_4Cl (μmol)	N_2H_5Cl (μmol)	Equiv NH_3/Fe	% Yield Based on H^+
A	2	2.3	[322]x2[a]	[162]x2	115.0	0.1	49.6	46.2
B	2	2.3	[322]x2[a]	[162]x2	145.6	0.0	62.8	58.5
Avg.							56 ± 9	52 ± 9
C	3	2.3	[322]x3[a]	[162]x3	182.4	0.3	78.7	48.9
D	3	2.3	[322]x3[a]	[162]x3	207.3	0.1	89.5	55.5
Avg.							84 ± 8	52 ± 5

[a]Acid used is [Ph_2NH_2][OTf]

5. Time-resolved H_2 quantification of background acid and Cp^*_2Co reactivity:

Inside of a nitrogen filled glovebox, solid acid (0.248 mmol) and Cp^*_2Co (0.124 mmol) are added to a 260 mL glass tube charged with a stir bar. The vessel is sealed with a septum at RT and subsequently chilled to -196 °C in a cold well in the nitrogen filled glovebox. Et_2O (1 mL) is added via syringe into the vessel and completely frozen. The vessel is passed out of the glovebox into a liquid N_2 bath, and subsequently thawed in a dry ice/acetone bath with stirring at ~900 rpm. The timer was started as soon as the vessel was transferred to the dry ice/acetone bath. The headspace of the reaction vessel was periodically sampled with a sealable gas sampling syringe (10 mL), which was loaded into a gas chromatograph, and analyzed for the presence of $H_{2(g)}$. From these data, the percent H_2 evolved (relative to Cp^*_2Co) was calculated, correcting for the vapor pressure of Et_2O and the removed H_2 from previous samplings. Each time course was measured from a single reaction maintained at -78 °C.

Table S6: Time-resolved H_2 quantification for the reaction of Cp^*_2Co and acid in Et_2O at -78 °C in the absence of an Fe precatalyst

Acid	Time (min)	$H_{2(g)}$ (μmol)	% H_2 Based on Cp^*_2Co
$[Ph_2NH_2][OTf]^a$	10	1.0 ± 0.4	1.6 ± 0.6
	60	2.1 ± 0.6	3 ± 1
$[Ph_2NH_2][BAr^F{}_4]^b$	10	3.7 ± 0.1	6.0 ± 0.2
	60	12.7 ± 0.8	21 ± 1

[a]Average of two experiments [b]Average of three experiments

6. Time-resolved NH_3 quantification:

All solvents are stirred with Na/K for ≥2 hours and filtered prior to use. In a nitrogen-filled glovebox, the precatalyst (2.3 μmol) was weighed into a vial. The precatalyst was then transferred quantitatively into a Schlenk tube using THF. The THF was then evaporated to provide a thin film of precatalyst at the bottom of the Schlenk tube. The tube is then charged with a stir bar and diphenylammonium triflate (108 eq) and decamethylcobaltocene (54 eq) are added as solids. The tube is then cooled to 77 K in a cold well. To the cold tube is added Et_2O to produce a concentration of precatalyst of 2.3 mM. The temperature of the system is allowed to equilibrate for 5 minutes and then the tube is sealed with a Teflon screw-valve. This tube is passed out of the box into a liquid N_2 bath and transported to a fume hood.

For the control reaction at this point a 2.6 M heptane solution of ^{t}BuLi (2 eq with respect to the acid) was added to the tube under N_2 backflow and the headspace was evacuated. The tube was then allowed to warm to room temperature with stirring and then stirred for a further ten minutes at room temperature. At this point the normal procedure was used to quantify NH_3 and N_2H_4. No NH_3 or N_2H_4 was observed.

To test catalytic activity at five minutes, a tube prepared as described above was allowed to stir for five minutes at -78 °C. At five minutes the tube was frozen in a liquid N_2 bath and allowed to equilibrate for five minutes. Under N_2 backflow a 2.6 M heptane solution of ^{t}BuLi (2 eq with respect to the acid) was added to the tube. The tube was then sealed and the headspace was evacuated. The reaction mixture was then allowed to warm to room temperature with stirring and then stirred for a further ten minutes at room temperature. At this point the normal procedure was used to quantify NH_3 and N_2H_4. Ammonia (1.2 ± 0.5 eq) was detected. No hydrazine was detected.

7. Mössbauer spectra:

7.1 General procedure for preparation of rapid-freeze-quench Mössbauer samples of catalytic reaction mixtures using $P_3{}^BFe^+$:

All manipulations are carried out inside of a nitrogen filled glovebox. The precatalyst, $[P_3{}^B(^{57}Fe)][BAr^F{}_4]$, is weighed into a vial (3.5 mg, 2.3 μmol) and transferred using THF into a 150 mL Schlenk tube. The solvent is evaporated to form a thin film of the precatalyst and a stir bar is added. The $[Ph_2NH_2][OTf]$ (79.4 mg, 0.248 mmol) and Cp^*_2Co (40.3 mg, 0.124 mmol) are added to the Schlenk tube as solids. The Schlenk tube is then placed in $N_{2(l)}$ and the temperature is allowed to equilibrate. To the tube 1 mL of Et_2O is added. The tube is then sealed with a Teflon screw tap and transferred to a pre-chilled cold well at -78 °C. The timer is set to zero as soon as the stir bar is freed from the thawing solvent. At the desired time, the tube is opened and the well-stirred suspension is transferred to a Delrin cup pre-chilled to -78 °C using a similarly pre-chilled pipette. The sample in the Delrin cup is then rapidly

frozen in $N_{2(l)}$. At this point the sample, immersed in $N_{2(l)}$, is taken outside of the glovebox and mounted in the cryostat.

7.2 General Procedure for Preparation of Rapid-freeze-quench Mössbauer Samples of the Reaction of $P_3^BFe^+$ with Reductants:

All manipulations are carried out inside of a nitrogen filled glovebox. The precatalyst, $[P_3^B(^{57}Fe)][BAr^F_4]$, is weighed into a vial (3.5 mg, 2.3 μmol) and .5 mL of THF is added. The solvent is then evaporated to provide a thin film of $[P_3^B(^{57}Fe)][BAr^F_4]$. To this is added the desired reductant as a solid (46.0 μmol, 20 equiv). This vial is then placed in $N_{2(l)}$ and the temperature is allowed to equilibrate. To this is added 1 mL of NaK-dried Et_2O. The vial is then sealed with a cap and transferred to a pre-chilled cold well at -78 °C. The timer is set to zero as soon as the stir bar is freed from the thawing solvent. After five minutes using a pre-chilled pipette the well-stirred reaction mixture is transferred to a Delrin cup that has been pre-chilled to -78 °C. The sample in the Delrin cup is then rapidly frozen in $N_{2(l)}$. At this point the sample, immersed in $N_{2(l)}$, is taken outside of the glovebox and mounted in the cryostat.

7.3 General Procedure for Fitting of Rapid-freeze-quench Mössbauer Samples:

Data analysis was performed using version 4 of the program WMOSS (www.wmoss.org) and quadrupole doublets were fit to Lorentzian lineshapes. Simulations were constructed from the minimum number of quadrupole doublets required to attain a quality fit to the data (convergence of χ_R^2). Quadrupole doublets were constrained to be symmetric, unless $[P_3^BFe–N_2][Na(12\text{-crown-}4)_2]$ was included in the model. With $[P_3^BFe–N_2][Na(12\text{-crown-}4)_2]$ since it is known to have characteristic asymmetry we started with the observed linewidths in the authentic sample and allowed them to then relax. It is known that the exact linewidths are sensitive to the particular sample but the relative line breadth should be fairly constant. Using the non-linear error analysis algorithm provided by WMOSS, the errors in the computed parameters are estimated to be 0.02 mm s^{-1} for δ and 2% for Δ_{Eq}. We additionally note that in these spectra the exact percentage contributions given do not represent exact percentages. Particularly for components that represent less than 10% of the overall spectrum, these values are subject to a high degree of uncertainty; however, all of the included components are necessary to generate satisfactory fits of the data and therefore are believed to be present in the reaction mixtures.

7.4. Details of Individual RFQ Mossbauer spectra:

Figure S2: Mössbauer spectrum collected on $P_3^B(^{57}Fe)^+$ that was used for the Mössbauer experiments conducted in this paper. The parameters used to model this species are well within the experimental error of those used previously to model this species (δ = 0.75 mm/sec, Δ_{Eq} = 2.55 mm/sec, $\Gamma_r = \Gamma_l$ = 0.52 mm/sec).

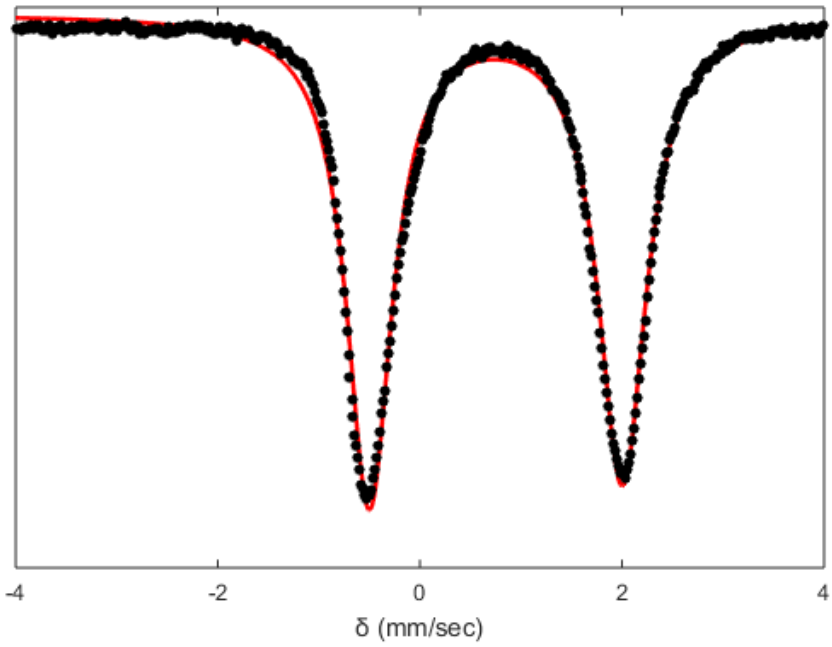

Table S7: Fit parameters for $(P_3^BFe^+)^{22}$

Component	δ (mm s^{-1})	ΔE_Q (mm s^{-1})	Linewidths, Γ_L/Γ_R (mm s^{-1})
Fit	0.75 ± 0.02	2.50 ± 0.05	0.54/0.58

Figure S3: Mössbauer spectrum collected from a reaction freeze quenched after 5 minutes between $P_3^BFe^+$ and excess Cp^*_2Co (20 equiv). Raw data shown as black points, simulation as a solid red line, with components in green, blue, yellow, and purple (see Table S8 for parameters). The spectrum was collected at 80 K with a parallel applied magnetic field of 50 mT as a suspension in Et_2O.

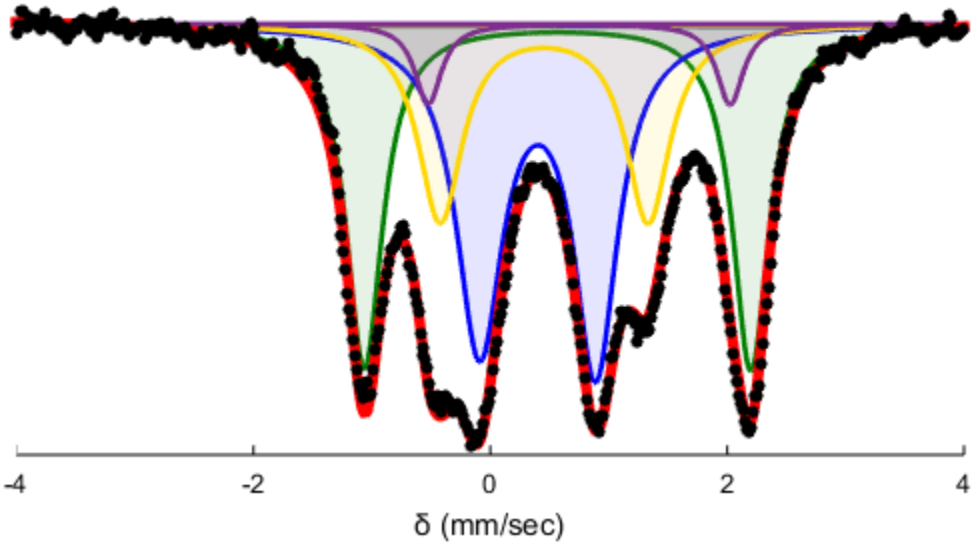

Fitting details for Figure S3: Four quadrupole doublets were found to be necessary to obtain an adequate simulation. The simulation parameters are given in Table S8. The two major species in this spectrum are well simulated as $P_3^BFe–N_2$ and $P_3^BFe–N_2^-$. The residual signal exhibits only two well resolved absorbances but to obtain a good fit with symmetric lineshapes two additional quadrupole doublets were necessary. One of these can be identified as $[P_3^BFe]^+$ based on the asymmetry in the lineshape of the right feature of $P_3^BFe–N_2$. The similarity of the other two quadrupole doublets to those identified in the five-minute freeze quench make this a logically consistent fit but one that is not strictly required by the data.

Table S8: **Simulation parameters for Mossbauer spectrum in Figure S3**

Component	δ (mm s^{-1})	ΔE_Q (mm s^{-1})	Linewidths, Γ_L/Γ_R (mm s^{-1})	Relative area
A (green)	0.57 ± 0.02	3.26 ± 0.06	0.29/0.29	0.33
B (purple)	0.75 ± 0.02	2.55 ± 0.05	0.27/0.27	0.06
C (yellow)	0.45 ± 0.02	1.76 ± 0.04	0.45/0.45	0.23
D (blue)	0.40 ± 0.02	0.98 ± 0.02	0.48/0.45	0.39

Figure S4: Mössbauer spectrum collected from a reaction freeze quenched after 5 minutes between $P_3^BFe^+$ and excess Cp^*_2Cr (20 equiv). Raw data shown as black points, simulation as a solid red line, with components in green and brown (see Table S9 for parameters). The spectrum was collected at 80 K with a parallel applied magnetic field of 50 mT as a suspension in Et_2O.

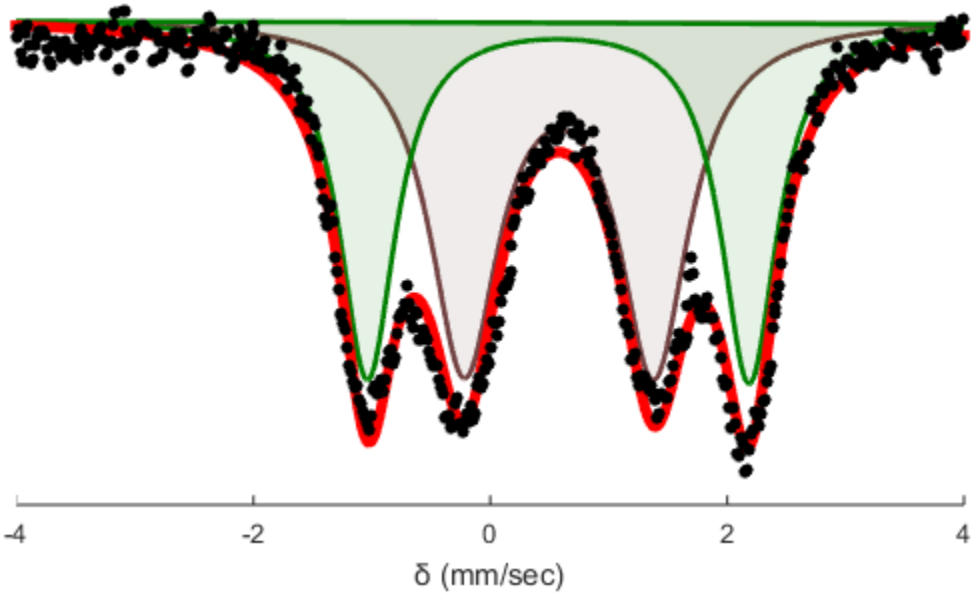

Fitting details for Figure S4: The two well-resolved quadrupole doublets can be simulated. The simulation parameters are given in Table S9. One of the two major species in this spectrum is well simulated as $P_3^BFe–N_2$. The other feature has a very similar isomer shift but a significantly narrower quadrupole splitting. Given the labile nature of the N_2 ligand this other species may represent a vacant neutral species or a dimeric N_2 bridged species.

Table S9: **Simulation parameters for Mossbauer spectrum in Figure S4**

Component	δ (mm s^{-1})	ΔE_Q (mm s^{-1})	Linewidths, Γ_L/ Γ_R (mm s^{-1})	Relative area
A (green)	0.57 ± 0.02	3.22 ± 0.06	0.29/0.29	0.46
B (brown)	0.58 ± 0.02	1.60 ± 0.05	0.71/0.71	0.54

Figure S5: Mossbauer spectrum collected from a catalytic reaction freeze quenched after 5 minutes. Conditions: [$P_3^B(^{57}Fe)$][BArF] = 0.23 mM, [Ph_2NH_2][OTf] = 24.8 mM (108 equiv), and Cp^*_2Co 12.4 mM (54 equiv). Raw data shown as black points, simulation as a solid red line, with components in green, blue, yellow, and orange (see Table S10 for parameters). The spectrum was collected at 80 K with a parallel applied magnetic field of 50 mT.

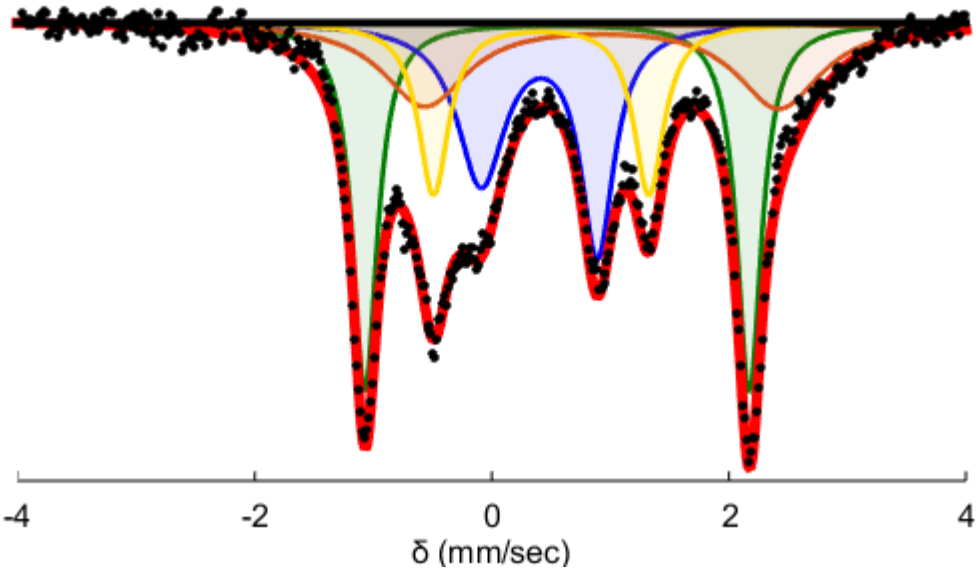

Fitting details for Figure S5: Four pairs of quadrupole doublets were found to be necessary to obtain an adequate simulation of these data. The simulation parameters are given in Table S10. The outer pair of sharp features clearly belong to $P_3^BFeN_2$. The inner feature is highly suggestive of $P_3^BFeN_2^-$ the presence of which was confirmed by freeze-quench EPR. The residual then consists of two sharp features which were simulated with the quadrupole doublet in yellow and a broader residual feature that is captured by the quadrupole doublet in orange. The exact isomer shift and quadrupole splitting of orange is not determined by this model but the one here is representative.

Table S10: Simulation parameters for Mossbauer spectrum in Figure S5

Component	δ (mm s^{-1})	ΔE_Q (mm s^{-1})	Linewidths, Γ_L/Γ_R (mm s^{-1})	Relative area
A (green)	0.55 ± 0.02	3.24 ± 0.06	0.25/0.25	0.32
B (blue)	0.40 ± 0.02	0.98 ± 0.02	0.49/0.34	0.26
C (yellow)	0.42 ± 0.02	1.82 ± 0.04	0.31/0.31	0.18
D (orange)	0.93 ± 0.02	2.99 ± 0.06	0.87/0.87	0.24

Figure S6: Mössbauer spectrum collected from a catalytic reaction freeze quenched after 30 minutes. Conditions: $[P_3^B(^{57}Fe)][BArF]$ = 0.23 mM, $[Ph_2NH_2][OTf]$ = 24.8 mM (108 equiv), and Cp^*_2Co 12.4 mM (54 equiv). Raw data shown as black points, simulation as a solid red line, with components in green, purple, yellow, and orange (see Table S11 for parameters). The spectrum was collected at 80 K with a parallel-applied magnetic field of 50 mT.

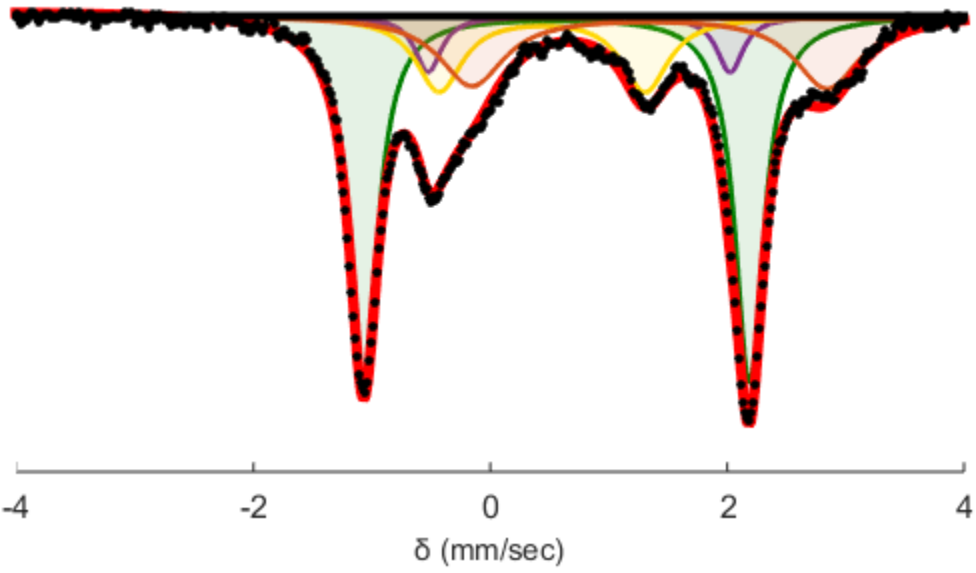

Fitting details for Figure S6: Four quadrupole doublets were found to be necessary to obtain an adequate simulation. The simulation parameters are given in Table S11. The major species in this spectrum is again well simulated as $P_3^BFe–N_2$. The residual signal exhibits only three well resolved absorbances. To obtain a good fit with symmetric lineshapes three additional quadrupole doublets were necessary. One of these can be identified as $[P_3^BFe]^+$ based on the asymmetry in the lineshape of the right feature of $P_3^BFe–N_2$. The similarity of the other two quadrupole doublets to those identified in the five-minute freeze quench make this a logically consistent fit but one that is not strictly required by the data.

Table S11: Simulation parameters for Mossbauer spectrum in Figure S6

Component	δ (mm s^{-1})	ΔE_Q (mm s^{-1})	Linewidths, Γ_L/Γ_R (mm s^{-1})	Relative area
A (green)	0.55 ± 0.02	3.24 ± 0.06	0.29/0.29	0.53
B (purple)	0.75 ± 0.02	2.55 ± 0.05	0.27/0.27	0.08
C (yellow)	0.44 ± 0.02	1.74 ± 0.04	0.48/0.48	0.18
D (orange)	1.35 ± 0.02	3.00 ± 0.06	0.67/0.67	0.22

8. EPR Spectra:

8.1 General Procedure for Preparation of Rapid-freeze-quench EPR Samples of Catalytic Reaction Mixtures using $P_3^BFe^+$:

All manipulations are carried out inside of a nitrogen filled glovebox. The precatalyst, $[P_3^BFe][BAr^F{}_4]$, is weighed into a vial (3.5 mg, 2.3 μmol) and transferred using THF into a 150 mL Schlenk tube. The solvent is evaporated to form a thin film of the precatalyst and a stir bar is added. The $[Ph_2NH_2][OTf]$ (79.4 mg, 0.248 mmol) and Cp^*_2Co (40.3 mg, 0.124 mmol) are added to the Schlenk tube as solids. The Schlenk tube is then placed in $N_{2(l)}$ and the temperature is allowed to equilibrate. To the tube 1 mL of Et_2O is added. The tube is then sealed with a Teflon screw tap and transferred to a pre-chilled cold well at -78 °C. The timer is set to zero as soon as the stir bar is freed from the thawing solvent. At the desired time, the tube is opened and the well-stirred suspension is transferred to an EPR tube that is prechilled to -78 °C using a pipette that has similarly been pre-chilled to -78 °C. The EPR sample is then rapidly frozen in $N_{2(l)}$. At this point the sample is quickly transferred out of the glovebox and put into $N_{2(l)}$ before it can warm.

8.2 General Procedure for Preparation of Rapid-freeze-quench EPR Samples of the Reaction of $P_3^BFe^+$ with Reductants:

All manipulations are carried out inside of a nitrogen filled glovebox. The precatalyst, $[P_3^BFe][BAr^F{}_4]$, is weighed into a vial (3.5 mg, 2.3 μmol) and .5 mL of THF is added. The solvent is then evaporated to provide a thin film of $[P_3^BFe][BAr^F{}_4]$. To this is added (46.0 μmol, 20 equiv) of the desired reductant as a solid. This vial is then placed in $N_{2(l)}$ and the temperature is allowed to equilibrate. To this is added 1 mL of NaK-dried Et_2O. The vial is then sealed with a cap and transferred to a pre-chilled cold well at -78 °C. The timer is set to zero as soon as the stir bar is freed from the thawing solvent. At the desired time, the tube is opened and the well-stirred suspension is transferred to an EPR tube that is prechilled to -78 °C using a pipette that has similarly been pre-chilled to -78 °C. The EPR sample is then rapidly frozen in $N_{2(l)}$. At this point the sample is quickly transferred out of the glovebox and put into $N_{2(l)}$ before it can warm.

8.3 General Procedure for Preparation of EPR Samples of Cp^*_2Co, $[P_3^BFe][BAr^F{}_4]$, and $[P_3^BFeN_2][Na(12\text{-crown-}4)_2]$:

The desired species was dissolved in 1 mL of Et_2O at RT and transferred to an EPR tube. The EPR tube was then chilled to -78 °C for five minutes. It was then rapidly frozen by transfer to a bath of $N_{2(l)}$.

8.4 Procedure for EPR Characterization of the Reaction of Cp^*_2Co with Acid:

The as isolated solid was added to a J-Young or septum-sealed X-Band EPR tube after prechilling both in the cold well to 77 K. Specific experimental details are listed with the accompanying spectra.

Figure S7: The X-band EPR spectrum in a 2-MeTHF glass of 2.3 mM $[P_3{}^BFe–N_2][Na(12\text{-crown-}4)_2]$ at 77K. Note that the exceeding insolubility of these species when encapsulated in a crown salt prevented its measurement in ether. We note that this species has significantly different parameters than the species in which the Na is not encapsulated with a crown ether and is therefore interacting with the N_2 ligand. We think this species is more representative of what a hypothetical $[P_3{}^BFe–N_2][Cp^*_2Co]$ species would look like if isolated.

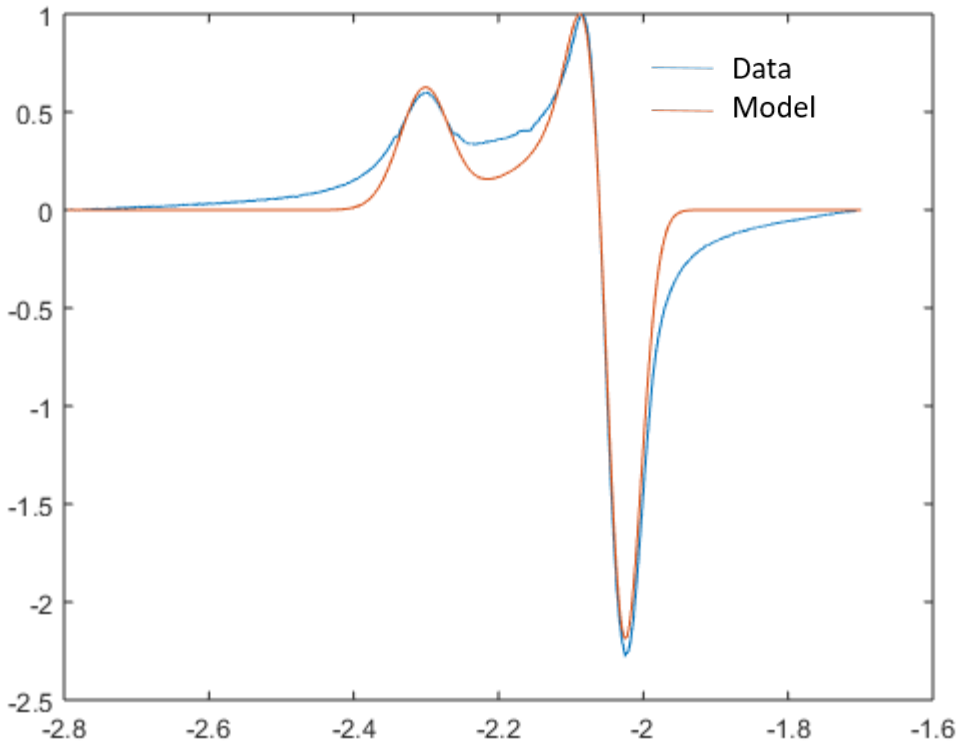

Figure S8: The X-band EPR spectrum in Et_2O of 2.3 mM $[P_3^BFe][BAr^F_4]$ at 77 K. Note this species is S = 3/2 and we have previously reported that this species is only observable at 10 K by X-band spectroscopy.[23] We attribute the extremely weak signal observed here to background signal from the cavity.

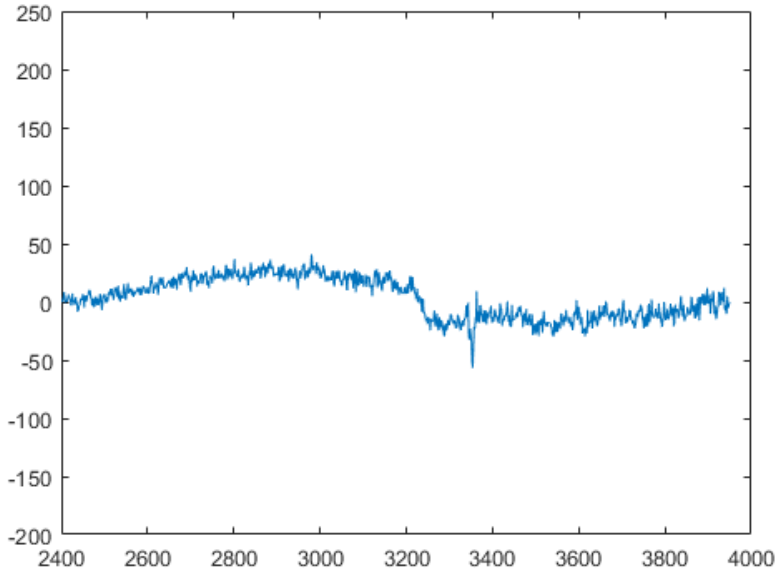

Figure S9: The X-band EPR spectrum in Et_2O of 46 mM Cp^*_2Co at 77K. Decamethylcobaltocene is known to be EPR silent at 77 K[24] but at these high concentrations it becomes apparent that there is a small S = ½ impurity present in this spectrum. This persistent impurity is observable in both freeze quenched reactions of this reductant with $[P_3^BFe][BAr^F_4]$ and in spectra of the freeze quenched catalytic reaction mixtures.

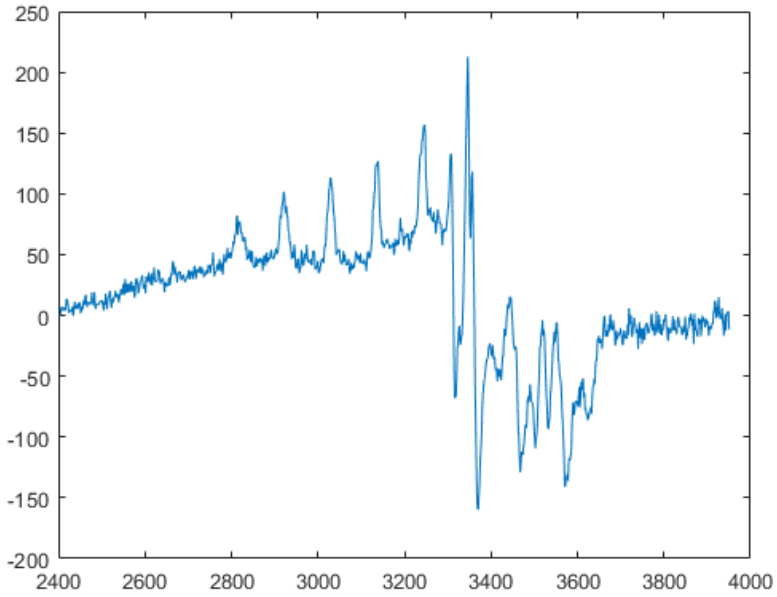

Figure S10: The X-band EPR spectrum in Et_2O (1 mL) of the reaction between $P_3{}^BFe^+$ (3.5 mg, 0.0023 mmol) and $Cp^*{}_2Co$ (15.2 mg, 0.046 mmol) stirred for 5 minutes at -78 °C then rapidly frozen to 77 K.

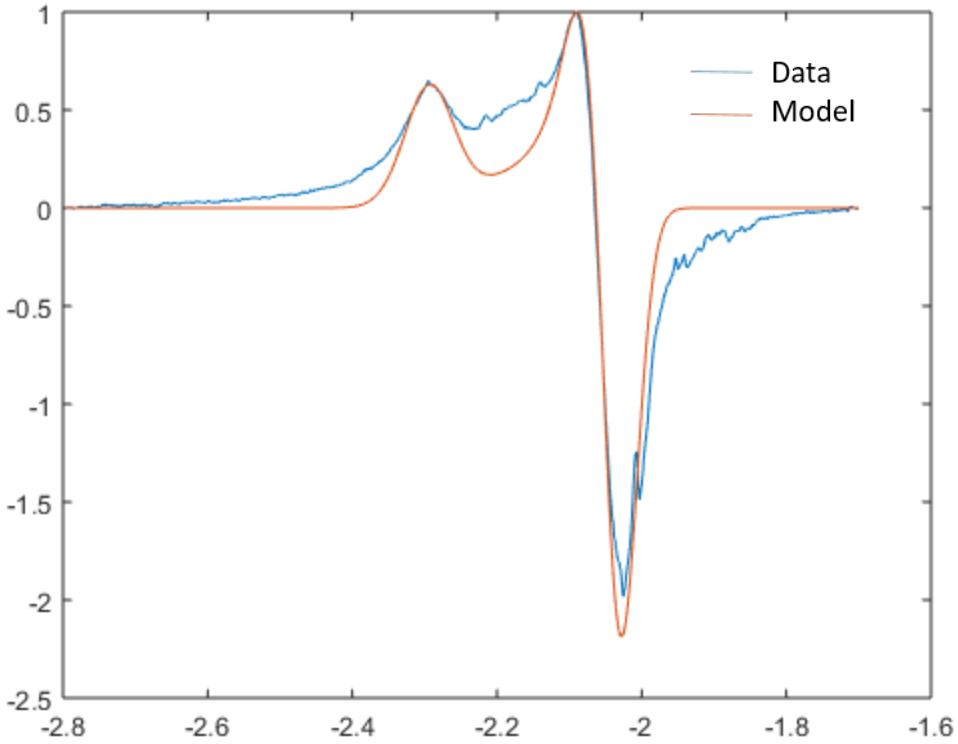

Figure S11: The X-band EPR spectrum in Et_2O (1 mL) of the reaction between $P_3^BFe^+$ (3.5 mg, 0.0023 mmol) and Cp^*_2Co (40.3 mg, 0.124 mmol) and $[Ph_2NH_2][OTf]$ (79.4 mg, 0.248 mmol) stirred for 5 minutes at -78 °C then rapidly frozen to 77 K.

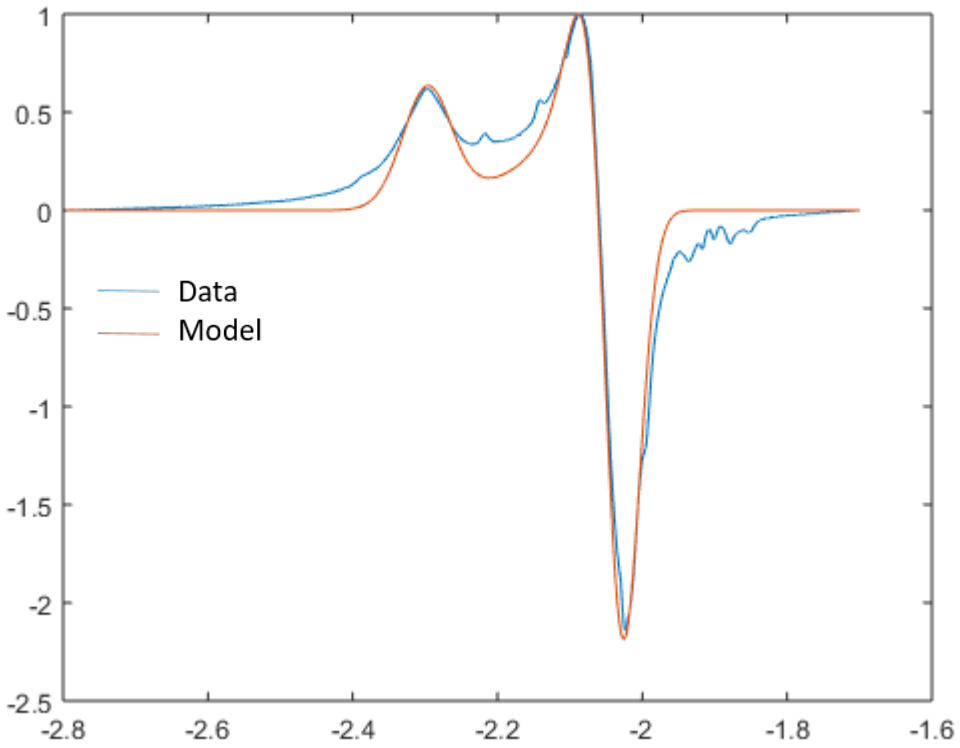

Table S12: **A comparison of the best fitting parameters for the authentic sample of $P_3^BFeN_2^-$ (A), the freeze quench of the reaction with the reductant (B), the freeze quench of the catalytic reaction mixture (C)**

Reaction	g_x	g_y	g_z
A	2.304	2.048	2.032
B	2.295	2.048	2.032
C	2.298	2.048	2.032

8.5 Discussion of the EPR spectra obtained by reacting Cp^*_2Co with Acid:

Previous studies have demonstrated that the EPR signal for Cp^*_2Co is only apparent at temperatures below the 77 K used in this study. In line with this expectation the solution spectra of Cp^*_2Co at 77 K do not show any signal (Figure S12, gren). The 77 K powder, X-band EPR spectrum obtained of the material isolated as described in SI 2.2 (Figure S12, red) demonstrates a signal with significant g-anisotropy and Co-hyperfine coupling. Although ^{1}H-hyperfine coupling is not resolved in this spectrum we believe that this is due to the large Co-hyperfine coupling and the significant linewidths observed (Figure S13). Attempts to obtain narrower linewidths by diluting the solid in KBr did not lead to any observable improvement. However, comparison of the spectrum obtained from reaction of Cp^*_2Co with HOTf and DOTf (Figure S14) strongly supports the hypothesis that this material represents a protonated Cp^*_2Co. In particular, the narrower lineshapes observed in the reaction with DOTf evidence both that the metallocene has been protonated but also that this proton is strongly coupled to the spin. The narrower line shapes manifest because of the lesser gyromagnetic ratio of ^{2}H compared to ^{1}H confirming that the linewidths in the reaction with HOTf are in part broadened by coupling to the added proton. That the appearance of the extra lines observed in the reaction with DOTf can be well-simulated simply by dividing the anisotropic strain parameter (HStrain in EasySpin) by the ratio of the ^{1}H gyromagnetic ratio:^{2}H gyromagnetic ratio (~6.5) strongly supports this hypothesis (Figure S15). That two species are present (more obvious in the DOTf reaction due to the sharper lineshapes) is further evidence that these spectra represent *endo*- and *exo*-protonated decamethylcobaltocene ($Cp^*Co(\eta^4\text{-}C_5Me_5H)^+$, as we would expect both the *endo*- and *exo*-protonated isomers to be kinetically and thermodynamically accessible under these conditions, and they should manifest distinct EPR signatures. Although preliminary in nature the observed reactivity of these species (discussed in SI 9.1-9.3) is further evidence that this material is competent for PCET reactivity as predicted by DFT.

Figure S12: 77 K X-band EPR spectrum of a toluene solution of Cp^*_2Co (green), 77 K powder X-Band EPR spectrum of the purple solid isolated from the reaction of Cp^*_2Co and HOTf as described in SI 2.2 (red), and 77 K powder X-Band EPR spectrum after annealing the EPR tube RT for two hours (blue)

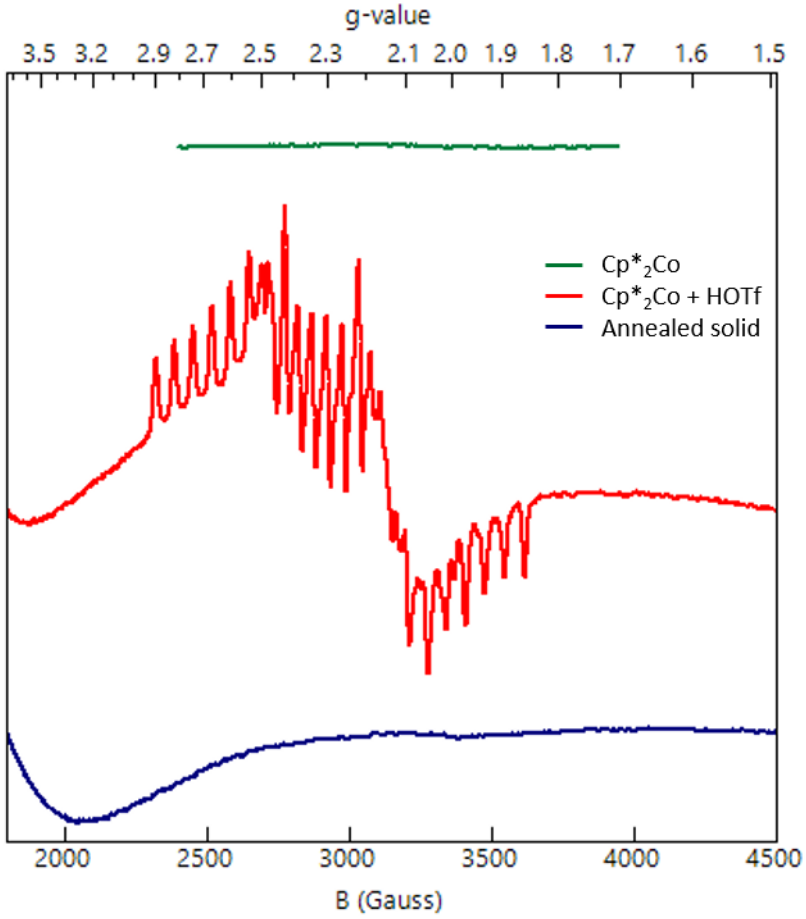

Figure S13: Powder EPR spectrum at 77 K for the reaction of HOTf and Cp^*_2Co and its simulation. Simulation parameters are g_1 = [2.63 2.345 1.984], $A_{1,Co}$ = [248 160 187], lw_1 = 1 MHz, $HStrain_1$ = [60 50 60], $Weight_1$ = 1; g_2 = [2.347 2.1 1.982], $A_{2,Co}$ = [200 50 110], lw_2 = 1, $HStrain_2$ = [40 40 40], $Weight_2$ = 0.2.

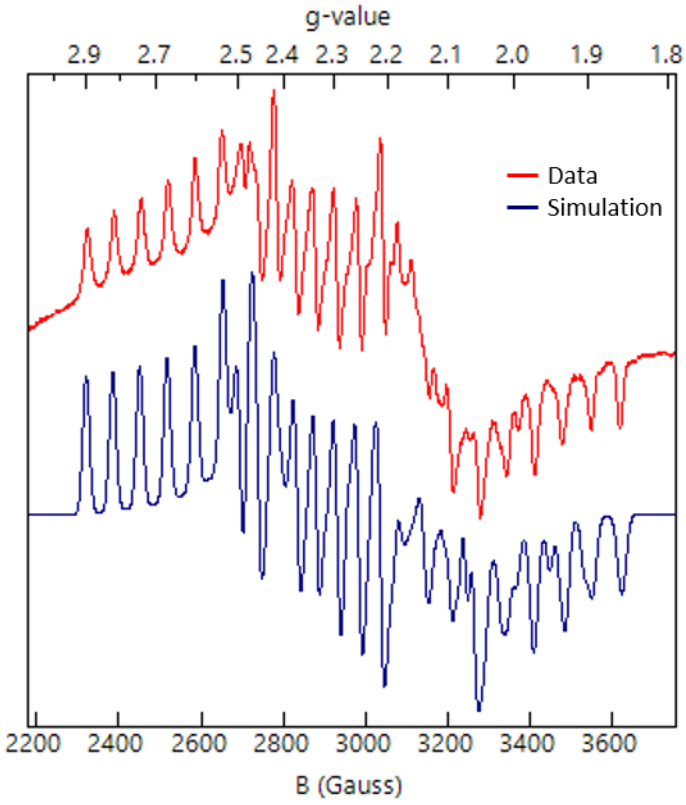

Figure S14: Comparison of the EPR spectra obtained using HOTf and DOTf in the reaction with Cp^*_2Co. The zoomed in spectrum highlights the middle g-value where the differences are most apparent between the two reactions.

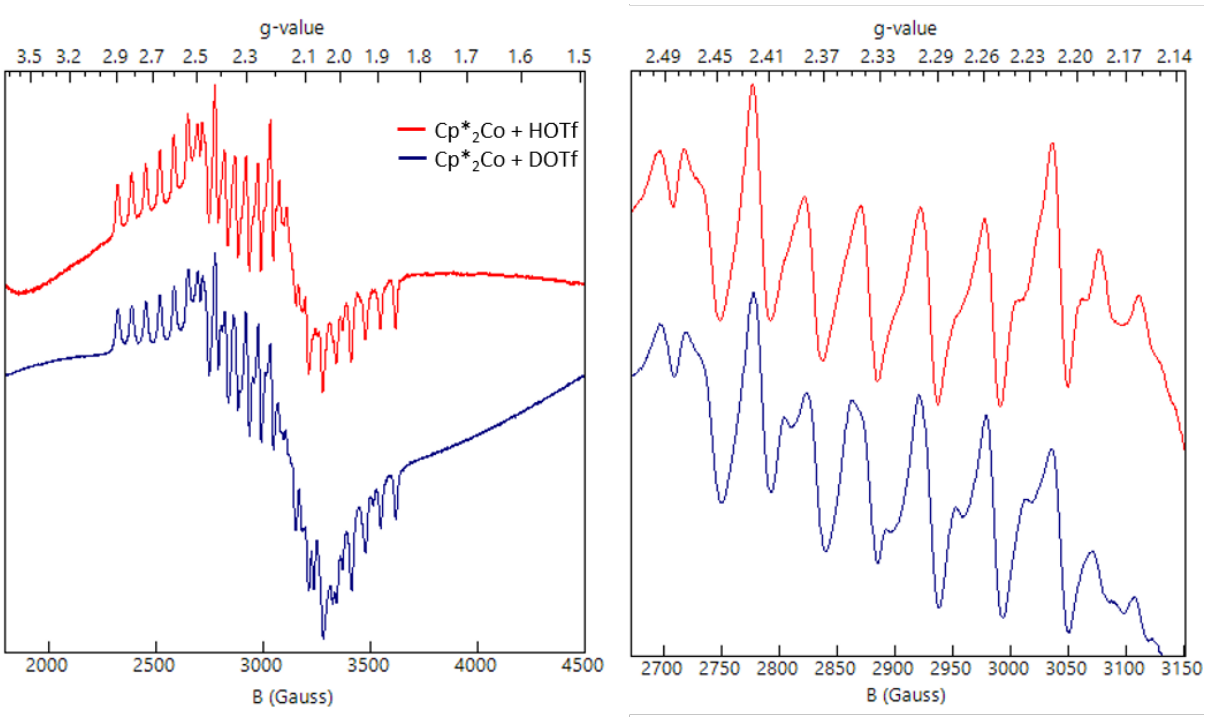

Figure S15: EPR spectrum obtained when reacting DOTf with Cp^*_2Co and its simulation. Simulation parameters are g_1 = [2.63 2.345 1.984], $A_{1,Co}$ = [248 160 187], lw_1 = 1 MHz, $HStrain_1$ = [9.2 7.7 9.2], $Weight_1$ = 1; g_2 = [2.347 2.1 1.982], $A_{2,Co}$ = [200 50 110], lw_2 = 1, $HStrain_2$ = [6.2 6.2 6.2], $Weight_2$ = 0.2.

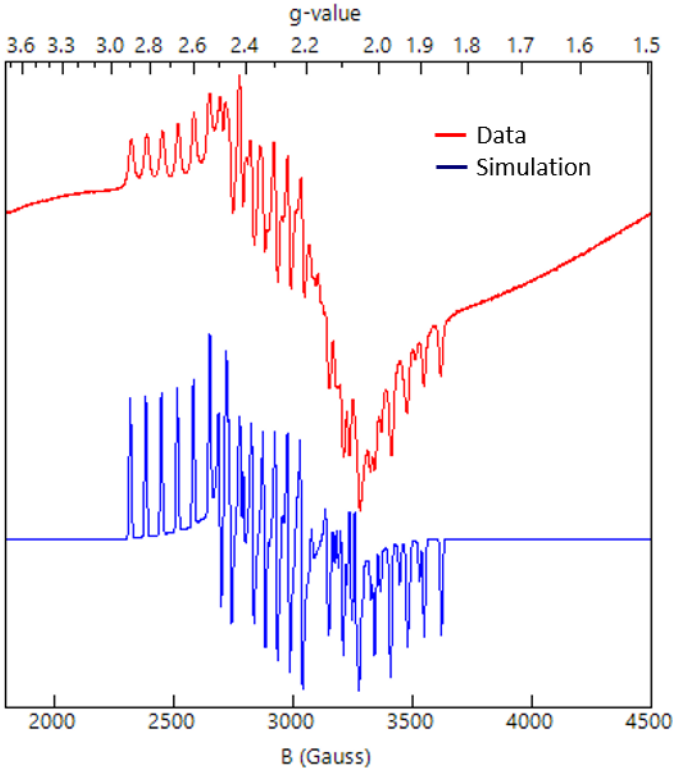

9. Reactivity of Cp*Co(η^4-C_5Me_5H)$^+$

9.1 Annealing Purple Solid:

Purple solid isolated as described in SI 2.2 was placed in an X-band EPR tube at 77 K and sealed with a rubber septum. A 77 K, powder X-band EPR spectrum was then taken to confirm the presence of Cp*Co(η^4-C_5Me_5H)$^+$. After two hours at room temperature a second 77 K, powder EPR spectrum was taken to confirm the quenching of Cp*Co(η^4-C_5Me_5H)$^+$. At this point the headspace was analyzed for H_2 via GC (14% yield).

9.2 Annealing Suspension of Purple Solid in Toluene:

Into a 26 mL vial with a septum seal was loaded 2 mL of toluene which was frozen at 77 K. To this purple solid isolated as described in SI 2.2 was added along with a stir bar. The suspension was stirred for 1 hour at −78 °C and then warmed to room temperature and stirred for an additional 15 minutes. At this point the headspace was sampled for H_2 via GC (35% yield). The solvent was then removed and to the yellow residue was added 1,3,5-trimethoxybenzene (1 eq.). The solid was then extracted with d_6-acetone and ^{1}H NMR was obtained. $Cp^*_2Co^+$ was observed (>95 % yield).

9.2 Upper Bound on Protonated Metallocene BDE

An upper bound for the BDE of the putative protonated metallocene was estimated using the literature BDE value for H_2 (105.8 kcal/mol) in MeCN, as well as the approximation for $T\Delta S_{H\cdot}$ (4.6 kcal/mol) in MeCN.[24] The maximum BDE was then approximated as follows:

$$\Delta G = \Delta H - T\Delta S < 0\,\frac{\text{kcal}}{\text{mol}}$$

$$\Delta H = BDE_{H2} - 2 * BDE_{Cp*2CoH+} = 105.8\,\frac{kcal}{mol} - 2 * BDE_{Cp*2CoH+}$$

$$T\Delta S = T\Delta S_{H\cdot} - 2 \cdot (T\Delta S_{H\cdot}) = -T\Delta S_{H\cdot} = -4.6\,\frac{kcal}{mol}$$

$$105.8\,\frac{kcal}{mol} - 2 * BDE_{Cp*2CoH+} + 4.6\,\frac{kcal}{mol} < 0\,\frac{kcal}{mol}$$

$$\therefore BDE_{Cp*2CoH+} < 50.6\,\frac{kcal}{mol}$$

10. Details on DFT Estimates of p*K*a and BDE

10.1 Computational Estimates of p*K*a in Et2O:

The pK_a values in diethyl ether were calculated referenced to $H(OEt_2)_2^+$ and were predicted on the basis of the free-energy change of the exchange reaction with $H(OEt_2)_2^+$ and application of Hess' law on the closed chemical cycle. The pK_a of $H(OEt_2)_2^+$ was defined as 0.0.

10.2 Computational Estimates of BDEs:

Bond dissociation enthalpies (BDE) of X–H bonds were calculated in the gas-phase using a series of known reference compounds containing M–OH, M–H and M–NH bonds.[20] The enthalpy difference between the H-atom donor/acceptor pair was calculated based on the thermochemical information provided by frequency calculations after structure optimizations using the procedure described in the general computational section. A linear plot of ΔH *vs* BDE_{lit} was generated to form a calibration curve (**Figure S12**). BDE predictions were generated by application of the line of best fit to the calculated ΔH of the unknown species. Error were calculated by application of the trend line to the calculated enthalpies of known species and comparison to their literature BDE value.[23] Errors are reported as the average of BDE_{calc}-BDE_{lit} (mean signed error, MSE) and the average of the absolute values of BDE_{calc}-BDE_{lit} (mean unsigned error, MUE). The use of the Bordwell equation for bond dissociation enthalpies is well supported by small $\Delta S_{calc} = S(X^{\bullet}) - S(XH)$, as shown in Table S14.

Table S13: Calculated ΔH values and literature BDE values used for BDE calibration

Species	ΔH_{calc}	BDE_{lit}	BDE_{calc}	Notes
$Cr(H_2O)_5(OH)^{2+}$	97.735	89	90	ref 25
$Fe(H_2O)_6^{2+}$	77.985	77	75	ref 25
$Cr(H_2O)_5(OOH)^{2+}$	77.175	79	75	ref 25
$bimFeN_2^{2+}$	69.255	67	68	ref 25
$P_3^{Si}Fe\text{-}C{=}NH^{+}$	65.905	65	66	ref 26
$bipFeH_2^{2+}$	65.475	62	65	ref 25
$TrenFeOH^{2-}$	64.105	66	64	ref 25
$CpFe(CO)_2H$	57.455	56	59	ref 25
$[HIPTN_3N]Mo\text{-}N{=}NH$	47.715	49	51	Truncated; ref 27
$P_3^{Si}Fe\text{-}N{=}NMeH^{+}$	43.915	48	48	ref 25
$P_3^{Si}Fe\text{-}C{=}NH$	38.915	44	44	ref 25
$P_3^{Si}Fe\text{-}C{=}NMeH$	34.375	45	40	ref 25
$P_3^{Si}Fe\text{-}C{=}NMeH^{+}$	32.955	44	39	ref 25
			MSE	-0.9
			MUE	2.1

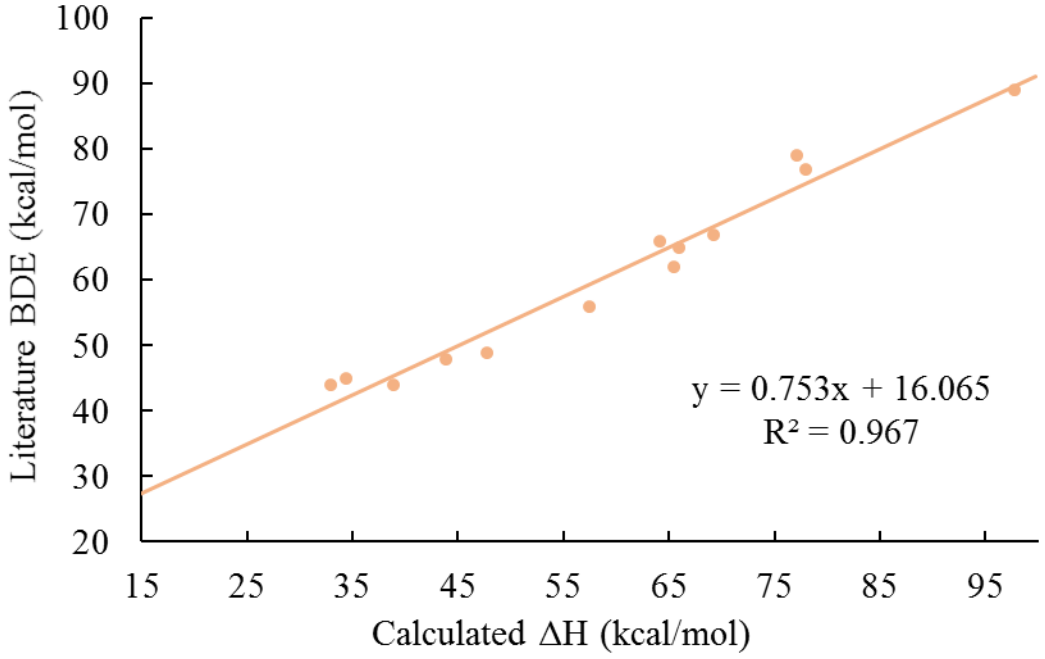

Figure S16: Calculated BDE vs literature BDE for the species shown in table S13.

Table S14: Calculated entropy (S) for selected XH and X• species

Species	S(X•) (cal/mol*K)	S(XH) (cal/mol*K)	ΔS (kcal/mol*K)
P_3^BFe-N=NH	271.6	268.9	$2.7x10^{-3}$
P_3^BFe=N-NH_2^+	266.3	273.1	$-6.8x10^{-3}$
P_3^BFe=N-NH_2	268.9	281.3	$-1.2x10^{-2}$
Cp*Co(η^4-C_5Me_5H)$^+$	168.8	162.0	$6.6x10^{-3}$
Cp*Cr(η^4-C_5Me_5H)$^+$	159.5	163.4	$-3.9x10^{-3}$

10.3 Estimation of PCET Activation Barriers:

Activation barriers were bracketed using the methods develop by the Hammes-Schiffer group. The inner sphere reorganization energy was estimated using force constants for normal modes in the Fe- and Co-coordination sphere.[28] The outer sphere reorganization energy (λ_{OS}) was estimated by calculating the outer sphere reorganization energy for a single ET in diethyl ether using the continuum solvation model[29] and assuming $\lambda_{OS,PCET} \leq \lambda_{OS,ET}$.[27] The activation barrier was plotted as a function of λ_{OS} (Figure S13) to determine a maximum and minimum barrier for each PCET reaction (Table S15).

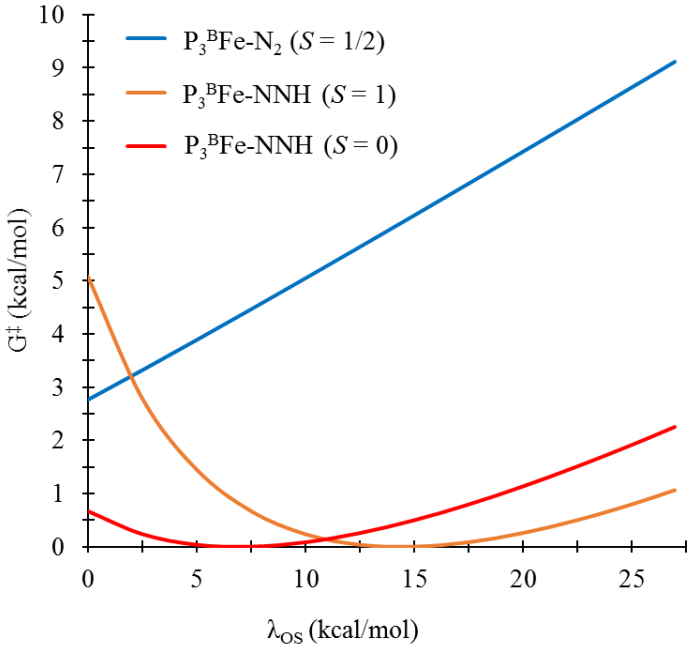

Figure S17: Activation barrier for PCET reactions between selected $P_3^BFe\text{-}N_xH_y$ species (as labeled, total spin-state of the surface in parenthesis) with $Cp^*Co(\eta^4\text{-}C_5Me_5H)^+$ as a function of outer-sphere reorganization energy.

Table S15: Calculated Reorganization Energies, Free-Energies of Reaction and Activation Barriers for Selected PCET Reactions

Acceptor	Spin State	Donor	λ_{tot} Range (kcal/mol)	ΔG_{rxn} (kcal/mol)	$G^‡$ Range (kcal/mol)
$P_3^BFe\text{-}N_2$	$S = ½$	$Cp^*Co(\eta^4\text{-}C_5Me_5H)^+$	26.1 - 53.5	-9.1	3 - 9
$P_3^BFe\text{-}NNH$	$S = 0$	$Cp^*Co(\eta^4\text{-}C_5Me_5H)^+$	17.7 – 45.1	-24.6	0 – 2
$P_3^BFe\text{-}NNH$	$S = 1$	$Cp^*Co(\eta^4\text{-}C_5Me_5H)^+$	10.2 – 37.6	-24.6	0 - 5

11. References:

1) Robbins, J. L.; Edelstein, N.; Spencer, B.; Smart, J. C. Syntheses and Electronic Structures of Decamethylmetallocenes. *J. Am. Chem. Soc.* **1982**, *104*, 1882–1893.

2) Anderson, J. S.; Moret, M.-E.; Peters, J. C. Conversion of Fe–NH2 to Fe–N2 with Release of NH3. *J. Am. Chem. Soc.* **2013**, *135*, 534–537.

3) Mankad, N. P.; Whited, M. T.; Peters, J. C. Terminal Fe-N2 and FeII···H-C Interactions Supported by Tris(phosphino)silyl Ligands. *Angew. Chem. Int. Ed.* **2007**, *46*, 5768–5771.

4) Del Castillo, T. J.; Thompson, N. B.; Suess, D. L. M.; Ung, G.; Peters, J. C. Evaluating Molecular Cobalt Complexes for the Conversion of N2 to NH3. *Inorg. Chem.* **2015**, *54*, 9256–9262.

5) Suess, D. L. M.; Tsay, C.; Peters, J. C. Dihydrogen Binding to Isostructural S = 1/2 and S = 0 Cobalt Complexes. *J. Am. Chem. Soc.* **2012**, *134*, 14158–14164.

6) Moret, M.-E.; Peters, J. C. Terminal Iron Dinitrogen and Iron Imide Complexes Supported by a Tris(phosphino)borane Ligand. *Angew. Chem. Int. Ed.* **2011**, *50*, 2063–2067.

7) Melzer, M. M.; Mossin, S.; Dai, X.; Bartell, A. M.; Kapoor, P.; Meyer, K.; Warren, T. H. A Three-Coordinate Copper(II) Amide from Reductive Cleavage of a Nitrosamine. *Angew. Chem. Int. Ed.* **2010**, *49*, 904–907.

8) Vicente, J.; Chicote, M.-T.; Guerrero, R.; Jones, P. G. Synthesis of Complexes [Au(PPh3)L]+(L = Primary, Secondary or Tertiary Amine). Crystal Structure of [Au(PPh3)(NMe3)][ClO4]·CH2Cl2. *J. Chem. Soc., Dalton Trans.* **1995**,*8*, 1251–1254.

9) Weatherburn, M. W. Phenol-Hypochlorite Reaction for Determination of Ammonia. *Anal. Chem.* **1967**, *39*, 971–974.

10) Watt, G. W.; Chrisp, J. D. Spectrophotometric Method for Determination of Hydrazine. *Anal. Chem.* **1952**, *24*, 2006–2008.

11) The Spin Count program developed by the Hendrich group at Carnegie Mellon was used to convert them to the g-value and then baseline them.

12) Stoll, S.; Schweiger, A. EasySpin, a Comprehensive Software Package for Spectral Simulation and Analysis in EPR. *Journal of Magnetic Resonance* **2006**, *178*, 42–55.

13) Zhao, Y.; Truhlar, D. G. A New Local Density Functional for Main-Group Thermochemistry, Transition Metal Bonding, Thermochemical Kinetics, and Noncovalent Interactions. *J. Chem, Phys.* **2006**, *125*, 194101: 1-18.

14) Weigend, F.; Ahlrichs, R. Balanced Basis Sets of Split Valence, Triple Zeta Valence and Quadruple Zeta Valence Quality for H to Rn: Design and Assessment of Accuracy. *Phys. Chem. Chem. Phys.* **2005**, *7*, 3297–3305.

15) Andrae, D.; Häußermann, U.; Dolg, M.; Stoll, H.; Preuß, H. Energy-Adjusted Ab Initio Pseudopotentials for the Second and Third Row Transition Elements. *Theoret. Chim. Acta* **1990**, *77*, 123–141.

16) *John Towns, Timothy Cockerill, Maytal Dahan, Ian Foster, Kelly Gaither, Andrew Grimshaw, Victor Hazlewood, Scott Lathrop, Dave Lifka, Gregory D. Peterson, Ralph Roskies, J. Ray Scott, Nancy Wilkins-Diehr, "XSEDE: Accelerating Scientific Discovery", Computing in Science & Engineering, vol.16, no. 5, pp. 62-74, Sept.-Oct. 2014, doi:10.1109/MCSE.2014.80*

17) Valiev, M.; Bylaska, E. J.; Govind, N.; Kowalski, K.; Straatsma, T. P.; Van Dam, H. J. J.; Wang, D.; Nieplocha, J.; Apra, E.; Windus, T. L.; de Jong, W. A. NWChem: A Comprehensive and Scalable Open-Source Solution for Large Scale Molecular Simulations. *Comput. Phys. Commun.* **2010**, *181*, 1477–1489.

18) Gaussian 09, Revision **B.01**, Frisch, M. J.; Trucks, G. W.; Schlegel, H. B.; Scuseria, G. E.; Robb, M. A.; Cheeseman, J. R.; Scalmani, G.; Barone, V.; Mennucci, B.; Petersson, G. A.; Nakatsuji, H.; Caricato,

M.; Li, X.; Hratchian, H. P.; Izmaylov, A. F.; Bloino, J.; Zheng, G.; Sonnenberg, J. L.; Hada, M.; Ehara, M.; Toyota, K.; Fukuda, R.; Hasegawa, J.; Ishida, M.; Nakajima, T.; Honda, Y.; Kitao, O.; Nakai, H.; Vreven, T.; Montgomery, J. A., Jr.; Peralta, J. E.; Ogliaro, F.; Bearpark, M.; Heyd, J. J.; Brothers, E.; Kudin, K. N.; Staroverov, V. N.; Kobayashi, R.; Normand, J.; Raghavachari, K.; Rendell, A.; Burant, J. C.; Iyengar, S. S.; Tomasi, J.; Cossi, M.; Rega, N.; Millam, J. M.; Klene, M.; Knox, J. E.; Cross, J. B.; Bakken,V.; Adamo, C.; Jaramillo, J.; Gomperts, R.; Stratmann, R. E.; Yazyev, O.; Austin, A. J.; Cammi, R.; Pomelli, C.; Ochterski, J. W.; Martin, R. L.; Morokuma, K.; Zakrzewski, V. G.; Voth, G. A.; Salvador, P.; Dannenberg, J. J.; Dapprich, S.; Daniels, A. D.; Farkas, Ö.; Foresman, J. B.; Ortiz, J. V.; Cioslowski, J.; Fox, D. J. Gaussian, Inc., Wallingford CT, 2009.

19) Ribeiro, R. F.; Marenich, A. V.; Cramer, C. J.; Truhlar, D. G. Use of Solution-Phase Vibrational Frequencies in Continuum Models for the Free Energy of Solvation. *J. Phys. Chem. B* **2011**, *115*, 14556–14562.

20) Wang, T.; Brudvig, G.; Batista, V. S. Characterization of Proton Coupled Electron Transfer in a Biomimetic Oxomanganese Complex: Evaluation of the DFT B3LYP Level of Theory. *J. Chem. Theory Comput.* **2010**, *6*, 755–760.

21) Marten, B.; Kim, K.; Cortis, C.; Friesner, R. A.; Murphy, R. B.; Ringnalda, M. N.; Sitkoff, D.; Honig, B. New Model for Calculation of Solvation Free Energies: Correction of Self-Consistent Reaction Field Continuum Dielectric Theory for Short-Range Hydrogen-Bonding Effects. *J. Phys. Chem.* **1996**, *100*, 11775–11788.

22) Anderson, J. S.; Cutsail, G. E.; Rittle, J.; Connor, B. A.; Gunderson, W. A.; Zhang, L.; Hoffman, B. M.; Peters, J. C. Characterization of an Fe≡N–NH2 Intermediate Relevant to Catalytic N2 Reduction to NH3. *J. Am. Chem. Soc.* **2015**, *137*, 7803–7809.

23) Anderson, J. S.; Moret, M.-E.; Peters, J. C. Conversion of Fe−NH_2 to Fe−N_2 with release of NH_3. *J. Am. Chem. Soc.* **2013**, *135*, 534-537.

24) Robbins, J. L.; Edelstein, N.; Spencer, B.; Smart, J. C. Synthesis and Electronic Structure of Decamethylmetallocenes. *J. Am. Chem. Soc.* **1982**, *104*, 1882-1893.

25) Warren, J. J.; Tronic, T. A.; Mayer, J. M. Thermochemistry of Proton-Coupled Electron Transfer Reagents and Its Implications. *Chem. Rev.* **2010**, *110*, 6961–7001.

26) Rittle, J.; Peters, J. C. N-H Bond Dissociation Enthalpies and Facile H-atom Transfers for Early Intermediates of Fe-N_2 and Fe-CN Reductions. *J. Am. Chem. Soc.* **2017**, DOI: 10.1021/jacs.6b12861.

27) Yandulov, D. V.; Schrock, R. R. Studies Relevant to Catalytic Reduction of Dinitrogen to Ammonia by Molybdenum Triamidoamine Complexes. *Inorg. Chem.* **2005**, *44*, 1103–1117.

28) Iordanova, N.; Decornez, H.; Hammes-Schiffer, S. Theoretical Study of Electron, Proton, and Proton-Coupled Electron Transfer in Iron Bi-Imidazoline Complexes. *J. Am. Chem. Soc.* **2001**, *123*, 3723–3733.

29) Marcus, R. A. On the Theory of Oxidation-Reduction Reactions Involving Electron Transfer. *J. Chem. Phys.* **1956**, *24*, 966–978.